KSTLE International Journal, Vol. 4, No. 1, June 2003, pp. 18-26

An Analysis of Dynamic Behavior of Fluid Dynamic Bearing for Hard Disk Drive Spindle Motor

Young-Han Song, Jin-Gyoo Yoo* and Yoon-Chul Rhim,†**

Department of Mechanical Eng. Graduate School, Yonsei University
**Storage Lab., Samsung Advanced Institute of Technology*
***School of Mechanical Eng., Yonsei University*

Abstract: Recently, fluid dynamic bearings (FDBs) have important applications in miniature rotating machines such as those found in the computer information storage industry, due to their outstanding low acoustic noise and NRRO (Non-Repeatable Run Out) characteristics. This research investigates the dynamic behavior of fluid dynamic bearings composed of hydrodynamic herringbone groove journal and spiral groove thrust bearing. The five degrees of freedom of FDB are considered to describe the real motion of a general rotor bearing system. The Reynolds equation and five nonlinear equations of motion for the dynamic behavior are solved simultaneously. The incompressible Reynolds equation is solved by using the finite element method (FEM) in order to calculate the pressure distribution in a fluid film and the five equations of motion by using the Runge-Kutta method. The reaction forces and moments are obtained by integrating the pressure along the fluid film. Numerical results are validated by comparing with the previously published experimental and numerical results. As a result, the dynamic behavior of FDB spindle such as orbit, floating height, and angular orbit is investigated by considering the conical motion under the static and dynamic load conditions.

Key words: Fluid dynamic bearing, herringbone groove journal bearing, thrust bearing, FDB, NRRO, dynamic behavior, FEM, orbit, spindle motor

Introduction

Recently, FDB is being considered as one of the better alternatives to conventional ball bearings for support of the rotating disk-spindle system in a HDD, due to its excellent vibration characteristics. It offers several distinctive advantages over the conventional ball bearing, including lower NRRO, lower acoustic noise and improved dynamic characteristics because the lubricant prevents direct contact between the rotating and the stationary parts and provides much higher damping. FDB can also be designed as leakage-free mechanical elements since the grooves have the ability to pump either with or against a pressure gradient and have the improved stability characteristics even at the concentric operation since the grooves can inhibit the whirl instability common to many self-acting journal bearings. In general, as shown in Fig. 1, FDB for the HDD spindle motor is composed of two herringbone groove journal bearings for support of the radial force and two spiral groove thrust bearings for support of the axial force.

The idea of using grooved surfaces in order to produce the pressure distribution in the bearing has been proposed by Whipple and is over 50 years old. Early analyses concentrated on the narrow groove theory (NGT) which assumes that the number of grooves approaches infinity. However, Bonneau and Absi [1] proved that the NGT is not accurate for the case of finite number of grooves. They showed the NGT overestimated the load performance of bearings with less than 16 grooves by using FEM. Zirkelback and San Andres [2] performed the parametric study of a HGJB for grooved member rotating to determine optimum dynamic force coefficients by using FEM.

Kang *et al.* [3] analyzed the dynamic characteristics of oil-lubricated groove journal bearing for the case of 8 grooves by using FDM and presented a novel manufacturing process for production of HGJB. Jang and Yoon [6] investigated the dynamic behavior of HGJB for both smooth and grooved

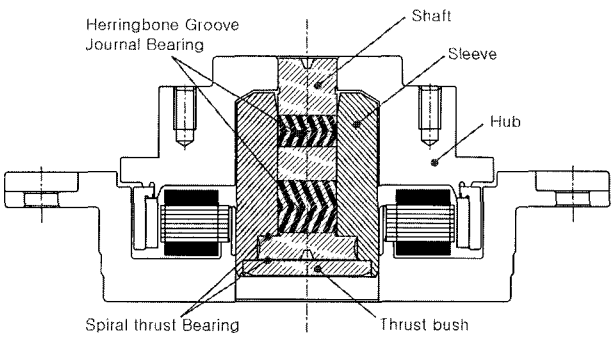

FDB spindle motor for HDD
(Untied type with rotary shaft)

Fig. 1. The schematic of FDB spindle motor for HDD.

†Corresponding author; Tel: 82-2-2123-2820, Fax: 82-2-312-2159
E-mail: ycrhim@bubble.yonse.ac.kr

member rotating under the static and dynamic load considering only the translation motion.

However, the above researchers analyzed the dynamic characteristics and behavior for the herringbone groove journal bearing and thrust bearing individually. In practice, FDB for the HDD spindle motor is composed of herringbone groove journal and thrust bearings. The new numerical method needs to be developed for analyzing the performance of the coupled herringbone groove journal and thrust bearing. Zang and Hatch [4], Rahman and Leuthold [5] presented the numerical method to analyze the coupled journal and thrust bearings system, and calculated the dynamic force coefficients by the translation motion of the coupled herringbone groove journal and thrust bearings. However, These studies were only concerned with the translation motion of the coupled journal and thrust bearings without considering the conical motion of the spindle at the steady state.

This paper investigates the dynamic behavior of fluid dynamic bearing composed of hydrodynamic herringbone groove journal and spiral groove thrust bearings considering five degrees of freedom to describe the real motion of a general rotor bearing system. The transient analysis of dynamic behavior is performed by solving simultaneously the Reynolds equation and five nonlinear equations of motion of a spindle. FEM and Runge-Kutta method is used to solve the Reynolds equation and five equations of motion, respectively.

Analysis

Governing Equation

Reynolds equation governs the pressure distribution of the fluid film in a hydrodynamic journal bearing, and for the incompressible fluid, it can be written in a fixed coordinate system as shown in Fig. 2.

$$\frac{1}{R^2}\frac{\partial}{\partial\Theta}\left(\frac{h^3}{12\mu}\frac{\partial p}{\partial\Theta}\right)+\frac{\partial}{\partial z}\left(\frac{h^3}{12\mu}\frac{\partial p}{\partial z}\right)=\frac{1}{2}\omega\frac{\partial h}{\partial\Theta}+\frac{\partial h}{\partial t} \tag{1}$$

where μ is the fluid viscosity, R is the journal radius, and ω is the angular velocity.

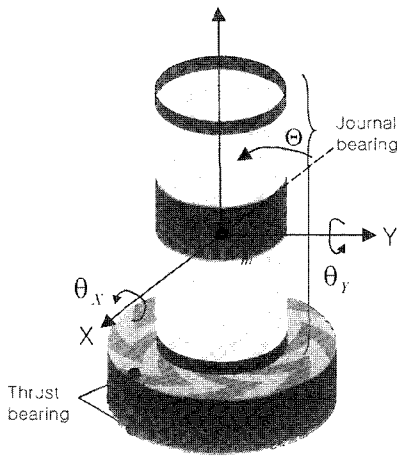

Fig. 2. Coordinate system of FDB.

The film thickness h can be expressed in terms of the translation motion and conical motion, and it can be written in the following form for the groove and land regions, respectively.

$$\begin{aligned} h &= c + c_g + e_X\cos\Theta + e_Y\sin\Theta + z'(\theta_Y\cos\Theta - \theta_X\sin\Theta) \\ h &= c + e_X\cos\Theta + e_Y\sin\Theta + z'(\theta_Y\cos\Theta - \theta_X\sin\Theta) \end{aligned} \tag{2}$$

where c and c_g are clearance and groove depth, respectively. z' is the axial distance from the center of mass (z_m). e_X and e_Y are the eccentricity in X and Y directions, and θ_X and θ_Y are the angular displacement by the conical motion.

When the smooth member rotates, the rotational motion of journal does not affect the rate of change of the film thickness. The rate of change of film thickness can be written as follows.

$$\frac{\partial h}{\partial t} = \dot{e}_X\cos\Theta + \dot{e}_Y\sin\Theta + z'(\dot{\theta}_Y\cos\Theta - \dot{\theta}_X\sin\Theta) \tag{3}$$

On the other hand, for the thrust bearing, Reynolds equation, film thickness and the rate of the film thickness can be written in following forms.

$$\frac{\partial}{r\partial r}\left(r\frac{h^3}{12\mu}\frac{\partial p}{\partial r}\right)+\frac{\partial}{r\partial\Theta}\left(\frac{h^3}{12\mu r}\frac{\partial p}{\partial\Theta}\right)=\frac{\omega}{2}\frac{\partial h}{r\partial\Theta}+\frac{\partial h}{\partial t} \tag{4}$$

$$\begin{aligned} h &= c + c_g + r(\theta_Y\cos\Theta - \theta_X\sin\Theta) \\ h &= c + r(\theta_Y\cos\Theta - \theta_X\sin\Theta) \end{aligned} \tag{5}$$

$$\frac{\partial h}{\partial t} = r(\dot{\theta}_Y\cos\Theta - \dot{\theta}_X\sin\Theta) \tag{6}$$

As shown in Fig. 2, FDB is composed of two herringbone groove journal bearings, two spiral groove thrust bearings and four oil reservoirs between bearings. The oil reservoir between each bearing is considered as a plain journal bearing with much larger clearance than the one of herringbone groove journal bearing. All parts are connected by the boundary condition that mass flow through the boundary is conserved.

After all, the pressure distribution of the whole bearing system is calculated by solving Eqs. (1), (2) and (3) for the journal bearings and Eqs. (4), (5) and (6) for thrust bearings by using FEM.

Boundary conditions for the coupled bearings system are the continuous pressure in the circumferential direction and the ambient pressure at the both sides of the whole bearing system, i.e., the inner boundaries of the lower thrust bearing and the upper side of the upper plain journal bearing. Half-Sommerfeld condition is applied to consider the cavitation.

Once the pressure is obtained, the reaction force and moment can be calculated as follows.

$$\begin{aligned} F_X &= \int_{journal part}\int p\cos\Theta R d\Theta dZ \\ F_Y &= \int_{journal part}\int p\sin\Theta R d\Theta dZ \\ F_Z &= \int_{journal part}\int p r dr d\Theta \end{aligned} \tag{7}$$

$$M_X = -\int_{journalpart}\int (z-z_m)p\sin\Theta R d\Theta dZ - \int_{journalpart}\int pr\sin\Theta r dr d\Theta$$

$$M_Y = -\int_{journalpart}\int (z-z_m)p\cos\Theta R d\Theta dZ - \int_{journalpart}\int pr\cos\Theta r dr d\Theta \quad (8)$$

Figure 3 shows the motion of five degrees of freedom of a spindle. They are made up of the translation motion in X, Y, and Z directions and the conical motion in Θ_x and Θ_y diretions. Under the external load and centrifugal force by the mass unbalance, the differentioal equations of motion of five degrees of freedom of the spindle can be written as Eqs (9) and (10). Equations (9) and (10) describe the translation motion and conical motion of the spindle, respectively.

The first terms on the right side of Eq. (9) are the bearing reaction forces in X, Y, and Z directions, and the second terms are the external load in in X, Y, and Z directions. The last terms are the centrifugal forces by the mass unbalance m_ue_u in X and Y directions, and η_0 is the phase angle of mass unbalance. The first terms on the right side of Eq. (10) for the conical motions are bearing reaction moments in Θ_x and Θ_y diretions, and the second terms are the external moments. The last terms are the moments by the axial eccentricity of mass unbalance from the center of mass, and z_u is the axial distacne of the mass unbalance.

$$\begin{aligned} m\ddot{e}_X &= F_X + W_X - m_u e_u \omega^2 \cos(\omega t + \eta_0) \\ m\ddot{e}_Y &= F_Y + W_Y - m_u e_u \omega^2 \sin(\omega t + \eta_0) \\ m\ddot{e}_Z &= F_Z + W_Z \end{aligned} \quad (9)$$

$$\begin{aligned} I_{XX}\ddot{\theta}_x &= M_X + M_{X_0} + (z_u - z_m) m_u e_u \omega^2 \sin(\omega t + \eta_0) \\ I_{YY}\ddot{\theta}_y &= M_Y + M_{Y_0} + (z_u - z_m) m_u e_u \omega^2 \cos(\omega t + \eta_0) \end{aligned} \quad (10)$$

Finite Element Formulation

FEM is used to solve the Reynolds equation for the coupled bearing system. The Reynolds equation is the second-order partial differential equation and can be written as follows.

$$A\frac{\partial^2 p}{\partial x_1^2} + B\frac{\partial p}{\partial x_1} + C\frac{\partial^2 p}{\partial x_2^2} + D\frac{\partial p}{\partial x_2} = E \quad (11)$$

where A, B, C, and D are the function of bearing geometry, and E is the wedge term and squeezing term of the Reynolds equation. The weighted residual equation is expressed as the following equations by using the Galerkin method.

$$\{R^{(e)}\} = -\int_A [N]^T \left(A\frac{\partial^2 p}{\partial x_1^2} + B\frac{\partial p}{\partial x_1} + C\frac{\partial^2 p}{\partial x_2^2} + D\frac{\partial p}{\partial x_2} - E \right) dA \quad (12)$$

where (e) denotes the element and $[N]^T$ is the column vector of element shape function. Equation (12) can be transformed to the weak form of Eq. (13) by using Green's theorem.

$$\begin{aligned} \{R^{(e)}\} = &-\int_\Gamma [N]^T \left(A\frac{\partial p}{\partial x_1}\cos\theta + C\frac{\partial p}{\partial x_2}\sin\theta \right) d\Gamma + \int_A A[N]^T dA \\ &+ \int_A \left(A\frac{\partial [N]^T}{\partial x_1}\frac{\partial p}{\partial x_1} - B\frac{\partial p}{\partial x_1} + C\frac{\partial [N]^T}{\partial x_2}\frac{\partial p}{\partial x_2} - D\frac{\partial p}{\partial x_2} \right) dA \end{aligned} \quad (13)$$

The pressure within each element can be approximated by its nodal values and shape functions.

$$p^{(e)} = [N]\{P^{\{e\}}\} \quad (14)$$

Substituting Eq. (14) into Eq. (13) gives

$$\begin{aligned} \{R^{(e)}\} = &-\int_\Gamma [N]^T \left(A\frac{\partial p}{\partial x_1}\cos\theta + C\frac{\partial p}{\partial x_2}\sin\theta \right) d\Gamma + \int_A E[N]^T dA \\ &+ \left[\int_A \left(A\frac{\partial [N]^T}{\partial x_1}\frac{\partial [N]}{\partial x_1} - B\frac{\partial [N]}{\partial x_1} + C\frac{\partial [N]^T}{\partial x_2}\frac{\partial [N]}{\partial x_2} - D\frac{\partial [N]}{\partial x_2} \right) dA \right] \{P^{\{e\}}\} \end{aligned} \quad (15)$$

Finally, the stiffness matrix and force vector for each bearing can be written in the following form.

$$\{k^{(e)}\} + \left[\int_A \left(A\frac{\partial [N]^T}{\partial x_1}\frac{\partial [N]}{\partial x_1} - B\frac{\partial [N]}{\partial x_1} + C\frac{\partial [N]^T}{\partial x_2}\frac{\partial [N]}{\partial x_2} - D\frac{\partial [N]}{\partial x_2} \right) dA \right]$$

$$\{f^{(e)}\} = -\int_A E[N]^T dA \quad (16)$$

The flow domain is discretized with the eight-noded quadratic finite elements, and the nine points Gauss-Legendre quadrature is used for the numerical integration. The algebraic matrix

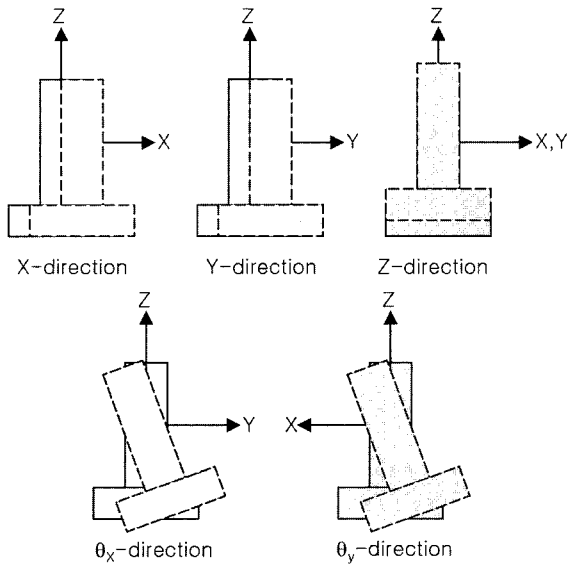

Fig. 3. Five degrees of freedom motion of the spindle.

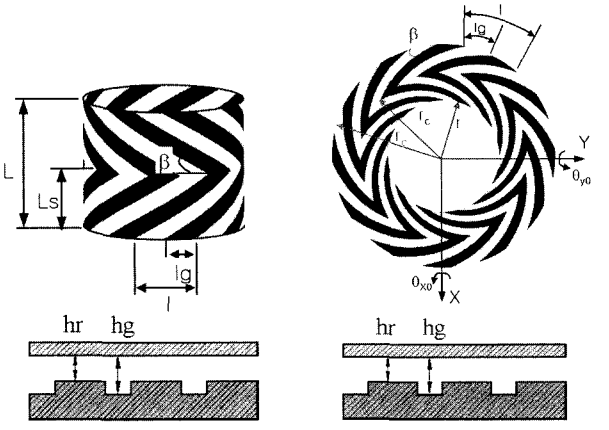

Fig. 4. Geometric parameters of HGJB and thrust bearing.

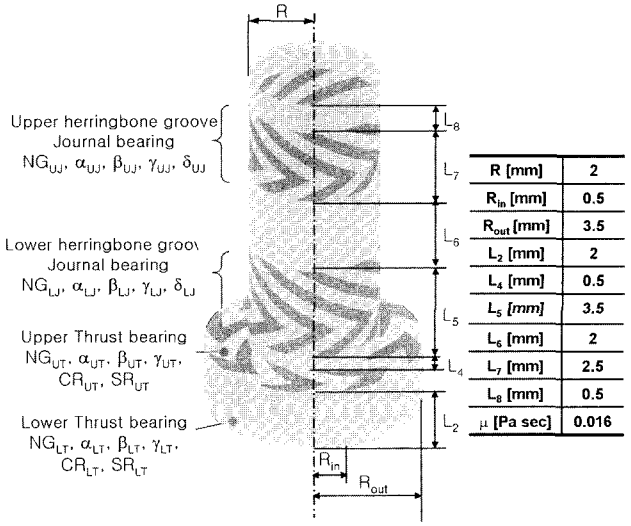

Fig. 5. Geometric parameters of FDB.

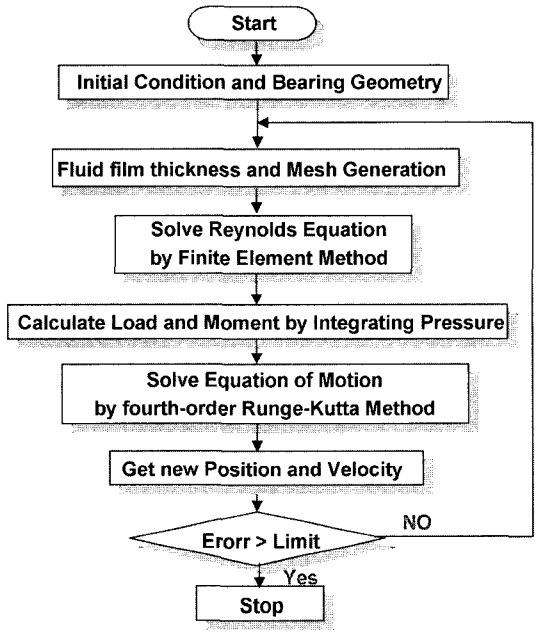

Fig. 6. Flow chart for dynamic behavior analysis of FDB system.

equations are solved by the skyline method.

Geometric parameters and Method of analysis

FDB has the herringbone and spiral grooves either on the moving surface or on the stationary surface. The grooves pump the lubricant inward thus generating support stiffness and improving its dynamic stability even at the concentric condition. Thus, the dynamic characteristics and behavior of FDB are mainly dependent on the geometry of grooves. Figure 4 shows the geometric parameters of herringbone groove journal and spiral groove thrust bearings which compose the FDB system.

Based on the definition of Fig. 4, Fig. 5 shows the schematic and geometric parameters of the coupled herringbone groove journal and spiral groove thrust bearings. The geometric parameters are a radius of the spindle R, an inner radius of the lower thrust bearing R_{in}, an outer radius of the lower thrust bearing R_{out}, a length of the spindle L, and the geometric parameters of each bearing defined previously. The subscript UJ and LJ represent the upper and lower journal bearing respectively, and UT and LT the upper and lower thrust bearing.

The computer program is developed to analyze the dymamic behavior of a HDD spindle motor with FDB system of Fig. 5 and the flow chart is shown in Fig. 6. At first, the mass, the center of gravity, and the moment of inertia are obtained for the rotating parts of FDB spindle motor mounted with two disks. The film thickness and mesh are generated with the initial conditions and the bearing geometry, and the Reynolds equation is solved by using FEM to calculate the pressure distribution in a fluid film with the initial conditions. Bearing reaction forces and moments are calculated by integrating the pressure along the fluid film. The five Equations of motion are solved by using the fourth-order Runge-Kutta method to obtain the new position and translational and conical velocity of the spindle. The numerical procedure is repeated until the spindle reaches the steady state and the periodic position.

Results and Discussion

In order to validate the present FEM model, the results obtained from the analysis are compared with the experimental and numerical results of the prior researchers. Figure 7 shows a comparison of the present numerical prediction with the experimental data presented by Hirs (1965) and the FEM results by Andres (1998). This numerical results show excellent correlation with the published results even at a high eccentricity ratio, and this clearly demonstrates the validity of the present analysis.

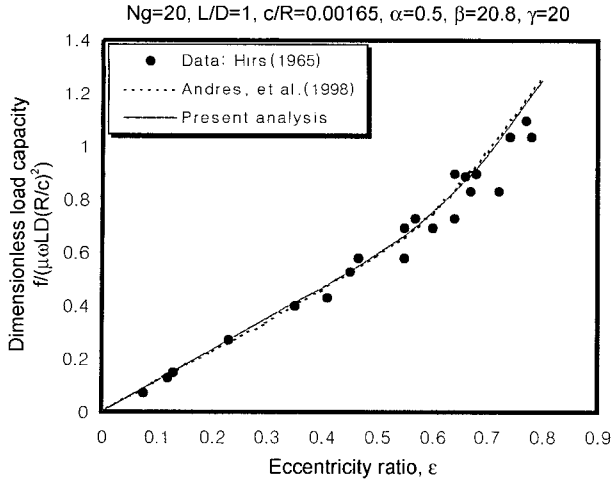

Fig. 7. Comparison of dimensionless load capacity with Hirs (1965) experimental data and Andres (1998) FEM data.

Geometric parameters

	UJ	LJ	UT	LT
NG	6	6	16	16
α	0.5	0.5	0.5	0.5
β	30	30	30	30
γ	2	2	2	2
δ	0.5	0.5		
CR			0.5	0.5
c_J	6 μm (clearance of journal)			
c_T	10 μm (clearance of thrust)			

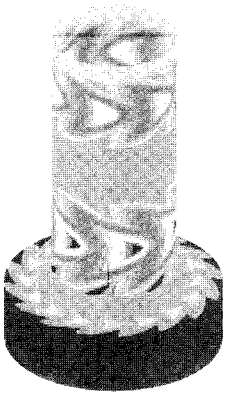

Fig. 8. Pressure contour of the coupled bearings system (e_x=e_y=0, e_z=10μm).

The pressure contour of the coupled bearings system is given in Fig. 8 at the X and Y directional eccentricity ratio of 0.0 and Z directional eccentricity ratio of 1.0. The geometric parameters of the coupled bearings system are shown in the left table of Fig. 8. Due to the smaller clearance of the journal bearings, the pressure of the journal bearings is higher than that of the thrust bearings. The pressure peak is generated at the central points of herringbone grooves and the turning points of spiral grooves, where the "central" and "turning" points form the intersection of grooves. Thus the number of pressure peak is equal to the number of grooves of each bearing at the concentric and aligned position.

Figures 10 through 12 show the comparisons of dynamic behavior considering and without considering the conical motions under the static and dynamic load conditions. The geometric parameters are listed and the rotational speed of the spindle is assumed, as shown in Fig. 9(a) and (b). The dynamic behavior considering and without considering the conical motion under the X directional static load (Wx = 5 N) is shown in Fig. 10. In case of the only translation motion without considering the conical motion, the spindle moves to the

Geometric parameters

	UJ	LJ	UT	LT
NG	8	8	8	8
α	0.5	0.5	0.5	0.5
β	30	30	30	30
γ	2	2	2	2
δ	0.5	0.5		
CR			0.5	0.5
c_J	6 μm (clearance of journal)			
c_T	10 μm (clearance of thrust)			

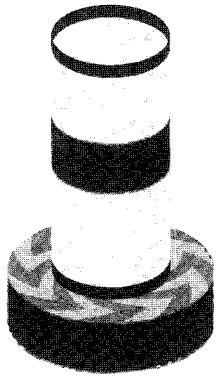

(a) Geometric parameters

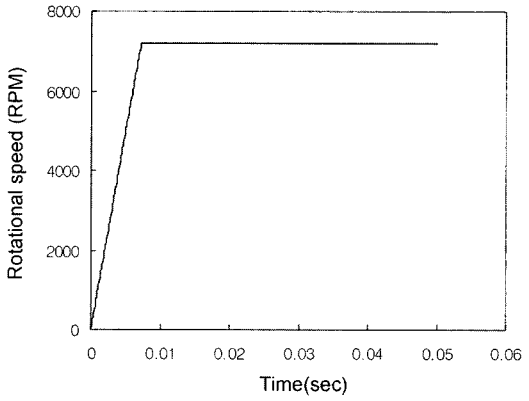

(b) RPM condition

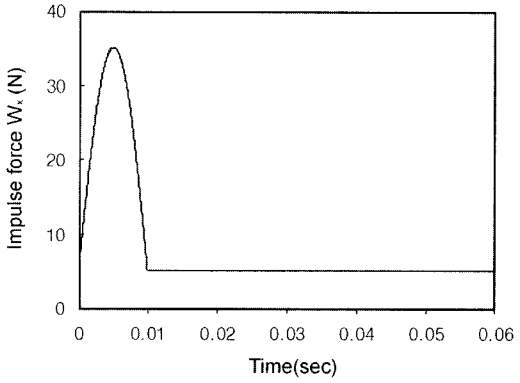

(c) Impulsive force condition

Fig. 9. Geometric parameters, RPM and impulsive force conditions for analysis.

positive X directional suddenly due to the static load, and moves slightly downward due to the weight of rotor. As the rotational speed increases, the bearing load capacity increases and the spindle converges to the fixed equilibrium position in X, Y and Z directions.

On the other hand, in case of the conical motion, the spindle misaligns to the positive Θ_y direction due to the moment by the pressure unbalance of axial direction, as shown in plot of the angular orbit, and then it converges to the fixed equilibrium position in Θ_x and Θ_y directions. Therefore, The motion of the spindle considering the conical motion shows a bigger trajectory and converges to the increasing equilibrium position

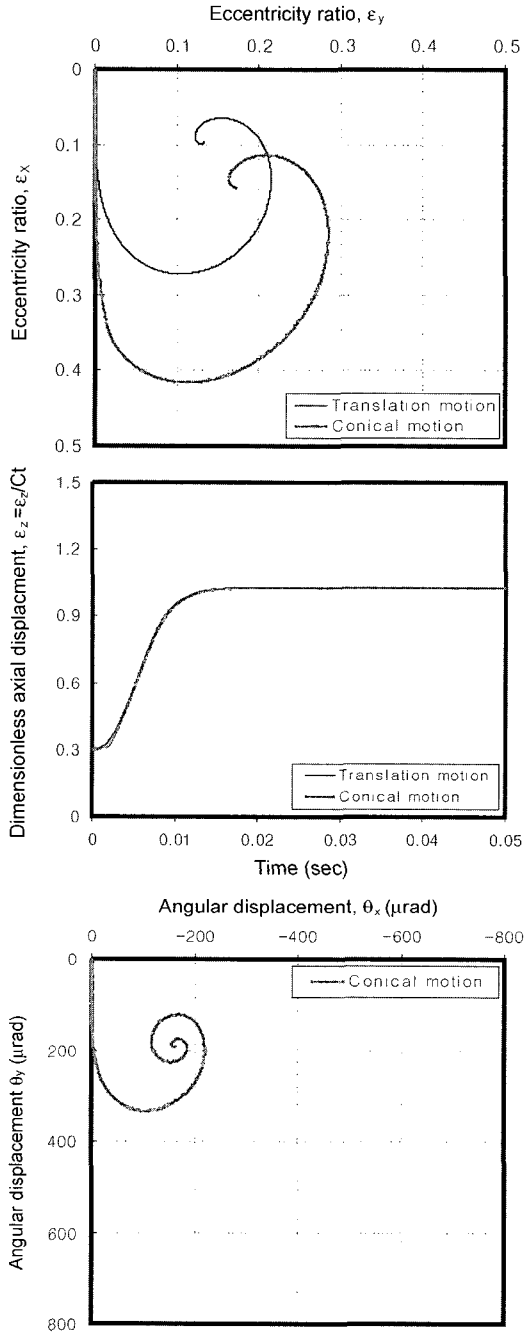

Fig. 10. Dynamic behavior of the spindle under the static load (Wx=5N).

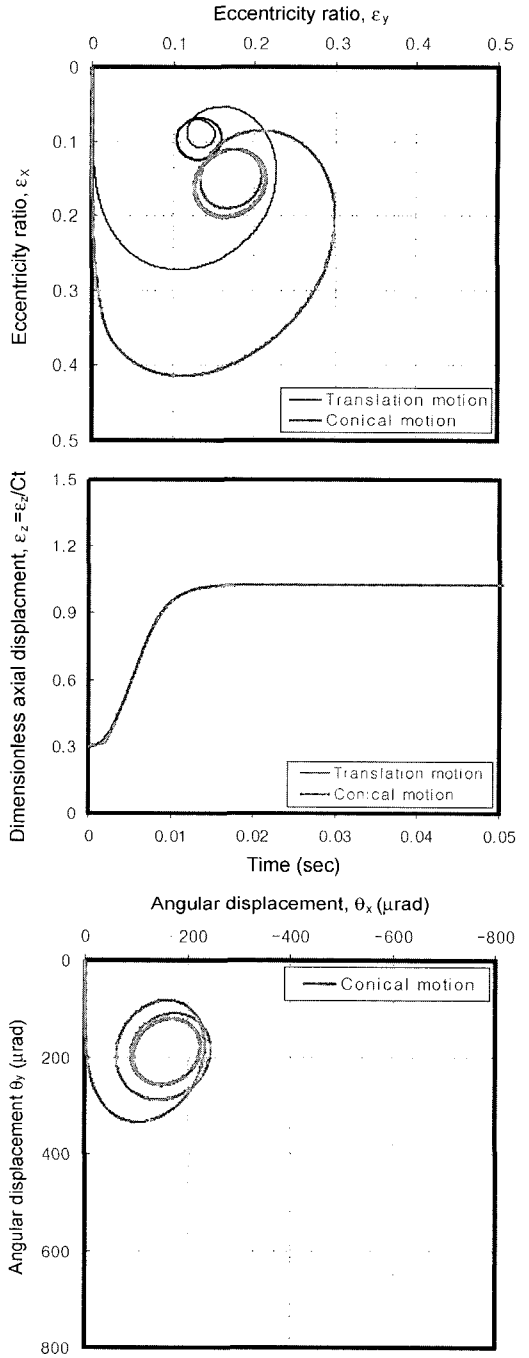

Fig. 11. Dynamic behavior of the spindle under the static load and mass unbalance (Wx=5 N, $m_u e_u$=134.8 mg · cm).

due to the misalignment of the spindle. However, the floating height is hardly influenced by the conical motion since the clearance of the thrust bearing is larger than that of the journal bearing.

Figure 11 shows the dynamic behavior considering and without considering the conical motion under the application of mass unbalance in addition to the static load. The mass unbalance is assumed to be 134.8mgcm, and it plays the role of the dynamic load in the form of centrifugal force. While the spindle reaches the steady state, its dynamic behavior is almost the same as the previous case. However, at the steady state, the mass unbalance produces the whirling motion not only in X and Y directions but also in Θ_x and Θ_y directions. The motion of the spindle considering the conical motion shows a bigger whirl than that of the spindle without considering the conical motion due to the misalignment of the spindle, but the floating height is hardly influenced by the conical motion as in the previous case.

Figure 12 shows the dynamic behavior considering and without considering the conical motion under the application of impulsive force at the equilibrium position of Fig. 10. The

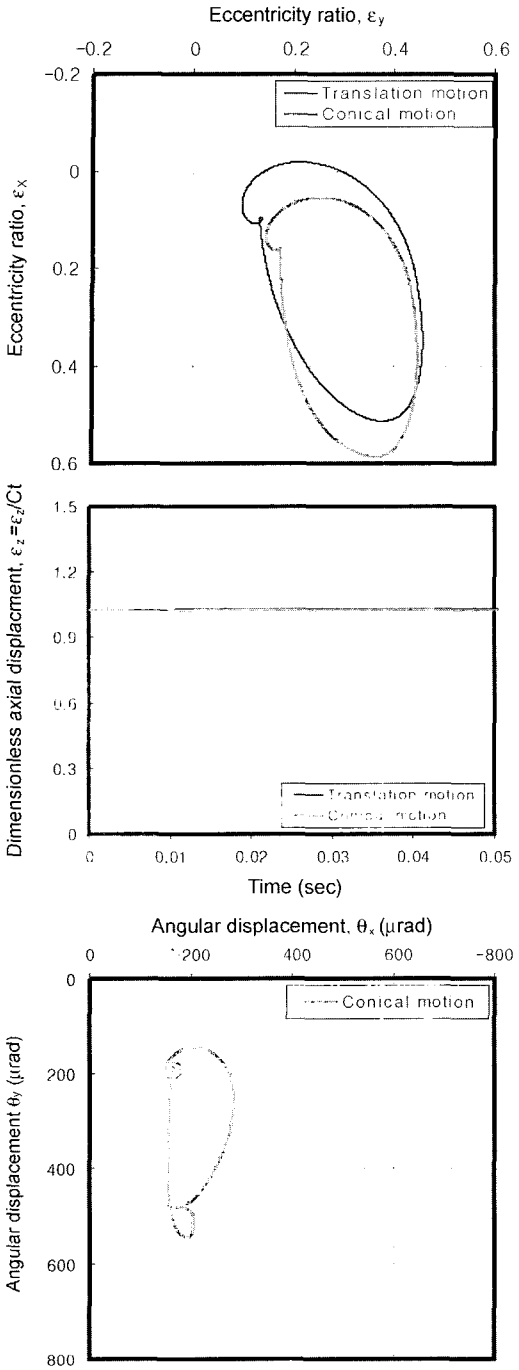

Fig. 12. Dynamic behavior of the spindle under the impulsive force.

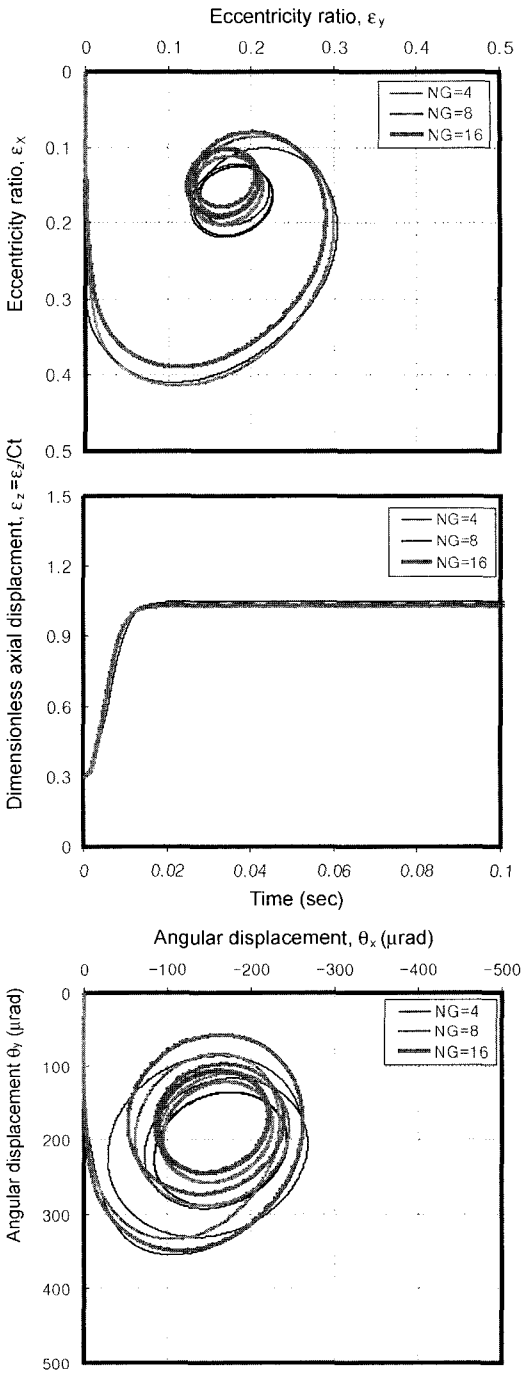

Fig. 13. Dynamic behavior of the spindle for number of grooves (Wx=5N, $m_u e_u$=134.8mg · cm).

impulsive force is assumed to be half sine wave, as shown in Fig. 9(c) and the rotational speed is 7200 RPM. The spindle moves to positive X direction with the increase of the impulsive force, and then it returns to the initial position with drawing an arc with the decrease of the impulsive force. In case of the conical motion, the floating height with respect to time has a small fluctuation and the spindle has the same trajectory as the translation motion in X and Y directions under the impulsive force.

From the above, the conical motion must be considered in the dynamic behavior analysis of FDB system because the spindle misaligns due to the pressure unbalance of axial direction in general rotor-bearing systems. The following results for the variation of the geometric parameters have considered the conical motion.

Figure 13 shows the dynamic behavior of the spindle for the number of grooves under the application of mass unbalance in addition to the static load. The geometric parameters and the rotational speed are given in Fig. 9(a) and (b). As the number of grooves increases, the orbit and angular orbit decrease. This

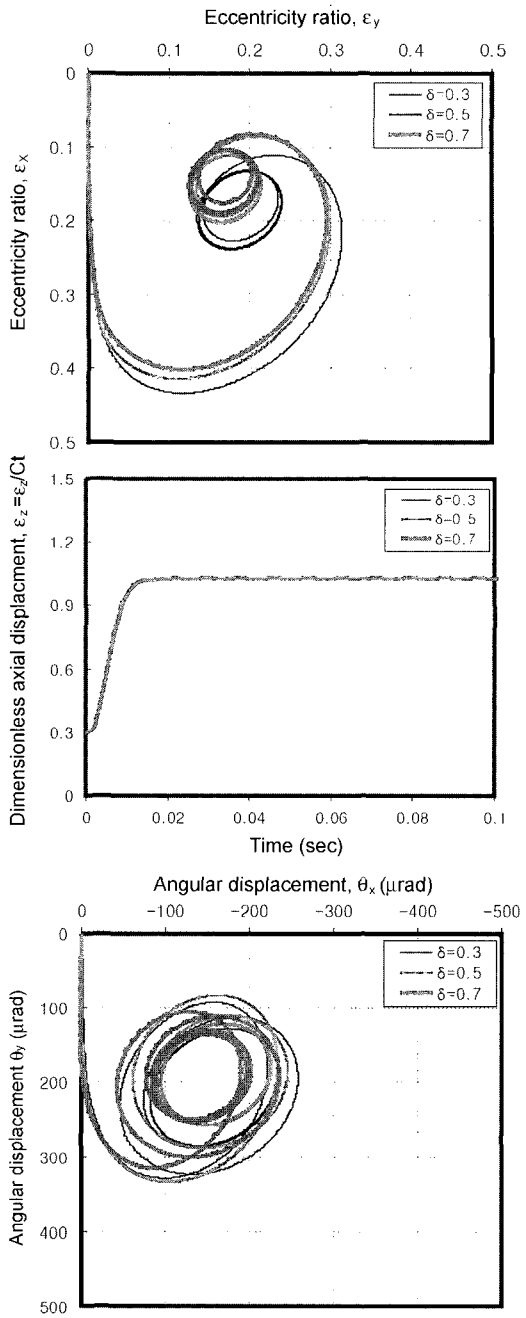

Fig. 14. Dynamic behavior of the spindle for asymmetric ratio of lower HGJB (Wx=5N, $m_u e_u$=134.8mg · cm).

is because the bearing load capacity increases with the increase of number of grooves. On the other hand, the floating height remains nearly unchanged with the increase of the number of grooves since the load capacity of the lower and upper thrust bearings increases together, but it acts on the spindle in the opposite direction.

The effects of the asymmetric ratio of the lower HGJB on the dynamic behavior are given in Fig. 14 under the application of mass unbalance in addition to the static load. The geometric parameters and the rotational speed are given in Fig. 9(a) and (b). As the asymmetric ratio increases, the axial distance from the center of mass to the central point of herringbone groove increases since the center of mass exists between the upper HGJB and the lower HGJB. Therefore, for the asymmetric ratio of 0.3, the spindle shows the biggest orbit and angular orbit, since the maximum moment acts on the spindle.

Conclusion

The transient analysis of dynamic behavior was performed for the coupled herringbone groove journal and thrust bearings system by solving simultaneously the Reynolds equation and five nonlinear equations of motion of a spindle considering the conical motion. The dynamic behaviors considering and without considering the conical motions make a great difference under the diverse load conditions. This is because the spindle misaligns due to the pressure unbalance of axial direction in general rotor-bearing systems as the conical motion is considered. Therefore, the conical motion must be considered in the dynamic behavior analysis of the coupled bearings system in order to describe accurately the motion of the spindle. Also, the dynamic behavior for the coupled bearings system was investigated for the variation of the geometric parameters. As the number of grooves and asymmetric ratio increase, the orbit and angular orbit become bigger, but the floating height remains nearly unchanged.

Acknowledgment

This work was funded by the Korea Science and Engineering Foundation (KOSEF) through the C storage Device (CISD) Grant No. R11-1997-042-12002-O.

References

1. Bonneau, D., and Absi, J., Analysis of Aerodynamic Journal Bearings with Small Number of Herringbone Grooves by Finite Element Method, ASME Journal of Tribology, Vol. 116, pp. 698-704, 1994.
2. Zirkelback, N., and Andres, L. S., Finite Element Analysis of Herringbone Groove Journal Bearings: A Parametric Study, ASME Journal of Tribology Vol. 120, pp. 234-240, 1998.
3. Kang, K., Rhim, Y., and Sung, K., Study of the Oil-Lubricated Herringbone Grooved Journal Bearing-Part 1: Numerical Analysis, ASME Journal of Tribology Vol. 118 pp. 906-911, 1996.
4. Yan Zan and Michael R. Hatch, Calculation of Dynamic Characteristics of Coupled Herringbone Journal and Thrust Hydrodynamic Bearing, Adv. Info. Storage Syst. Vol. 7, pp. 115-126, 1996.
5. Rahman, M., and Leuthold, H., Computer Simulation of a Coupled Journal and Thrust Hydrodynamic Bearing using a Finite-Element Method, IMCSD Proceedings, pp. 103-112, 1996.
6. Jang, G. H., and Yoon, J. W., Nonlinear Dynamic Analysis of a Hydrodynamic Journal Bearing Considering the Effects of a Rotating or Stationary Herringbone Groove, ASME Journal of Tribology, Vol. 124, pp. 297-304, 2002.
7. Hirs, G. G., The Load Capacity and Stability Characteristics of Hydrodynamic Grooved Journal Bearings, ASLE

Transactions, Vol. 8, pp. 296-305, 1965.
8. Oh, S. M., and Rhim, Y. C., The Numerical Analysis of Spindle Motor Bearing Composed of Herringbone Groove Journal and Spiral Groove Thrust Bearing, KSTLE International Journal, Vol. 2, No. 2, pp. 93-102, 2001.